

Role of weak uncorrelated pinning introduced by BaZrO₃ nanorods at low-temperature in (Y,Gd)Ba₂Cu₃O_x thin films

A. Xu,^{1,*} V. Braccini,² J. Jaroszynski,¹ Y. Xin,¹ and D. C. Larbalestier¹¹*Applied Superconductivity Center, National High Magnetic Field Laboratory, 2031 E. Paul Dirac Dr., Tallahassee, Florida 32310, USA*²*CNR-SPIN, Corso Perrone 24, I-16152 Genova, Italy*

(Received 21 October 2011; published 13 September 2012)

REBa₂Cu₃O_x (REBCO) films can achieve remarkably high critical current density J_c values by the incorporation of insulating nanoparticles. A particularly interesting case concerns BaZrO₃ (BZO) nanorods which strongly enhance J_c at high temperatures and fields up to a few tesla. Here we investigate the full angular transport J_c over a much broader range of field (up to 31 T) and temperature (4.2–77 K), a range suitable for new very high field magnet applications. We show that the correlated c -axis pinning of BZO nanorods becomes progressively less obvious at lower temperatures and indeed at 4.2 K up to 31 T, the only visible correlated pinning is for fields parallel to the film plane. J_c at 4.2 K is still, however, strongly enhanced by the BZO nanorods, as is clearly manifested by a remarkably high bulk pinning force density $F_p \approx 900$ GN/m³ for $H \parallel c$, because the BZO nanorods add weak but very dense pins which contribute up to half of J_c in the low temperature limit. Above about 30 K these dense but weak pins lose their effectiveness and J_c then becomes dominated by the sparse but strong BZO pins. This strong temperature dependence of the dominant pinning effects of multiple pin types makes broad range characterization essential to reveal the great flexibility of pinning in modern REBCO films that is almost certainly not yet fully optimized.

DOI: 10.1103/PhysRevB.86.115416

PACS number(s): 74.25.Wx, 74.25.Sv, 74.78.-w, 74.72.-h

I. INTRODUCTION

REBa₂Cu₃O_x (REBCO, where RE = rare earth) thin films with high supercurrent-carrying capability and low anisotropy remain strongly desirable for electronic, power, and magnet applications.^{1–3} The enhancement of critical current density J_c and modification of the angular dependence of J_c by the incorporation of second phases based on the understanding of vortex physics is a routine practice for REBCO thin films.^{4,5} In general, the maximum J_c of any superconductor is limited by the depairing current density J_d according to anisotropic Ginzburg-Landau theory.⁶ In fact REBCO films can clearly exert strong pinning, as shown by estimates that $\sim 30\%$ of J_d can be achieved by antiphase domain boundaries (APBs) in YBCO thin films grown on vicinal substrates, at least in low magnetic fields.⁷ Recently, the development of all-superconducting magnets above 25 T at 4.2 K became feasible,^{3,8} and some prototypes greater than 35 T were demonstrated.⁹ Efficient coil design depends on understanding the detailed angular dependence of J_c over broad temperature and magnetic field ranges. Because of the practical value of REBCO thin films in coated conductor form for such magnets, there is great interest in whether there still remain large opportunities for J_c enhancement at high fields where the vortex density is very high. Understanding what pins can give large effects at low temperatures and high magnetic fields is thus important both scientifically and technologically.

Previous studies of vortex physics in REBCO thin films mostly concentrated on the high temperature (77 K) and low magnetic field (0–3 T) regime. In this regime, elementary pinning forces are strong and the densities of pins and vortices are comparable. In addition to the strong low-field effect of APBs examined by Jooss *et al.*,⁷ it has been well documented that while uncorrelated pins, including Y₂BaCuO₅,¹⁰ RE₂O₃,^{5,11} and BZO nanoparticles^{12,13} are effective pins in a broad

angular range, correlated pins, including nanorods,^{14–17} RE₂O₃ precipitate arrays,¹⁸ and stacking faults^{19,20} make an even stronger but generally angularly selective contribution to J_c and, especially in the case of BZO nanorods, strongly enhance J_c in the high temperature regime where thermal depinning effects are strong and weak pins no longer operate. The lower temperature, very high field regime is thus interesting because smaller, weaker but perhaps denser pins that are thermally depinned at higher temperature could become important. Experimentally, however, transport J_c characterization in the low temperature, high field, and high current regime is much more difficult to perform and so little work has been done so far.

Many vortex pinning physics studies of REBCO thin films at lower temperatures have been previously reported,^{12,21–23} though in all cases the field regime has been below 10 T. Initially it was assumed that general conclusions could be drawn because it was tacitly supposed films were similar, but recent work has shown that an enormous variety of important flux pinning defects can be incorporated into REBCO films, making new investigations of vortex pinning with detailed nanostructure knowledge desirable. A common characterization has been through measurement of the power-law falloff of $J_c(H \parallel c)$ in the lower field range. Dam *et al.*^{24,25} reported that the power-law exponent is $\alpha \approx 0.5$ in YBCO thin films possessing screw dislocation growth spirals that act as strong correlated c -axis pinning defects which can plastically deform the flux lattice. In the case of REBCO thin films containing uncorrelated RE₂O₃ pins, Ijaduola *et al.*²¹ reported $\alpha \approx 5/8$ and compared their results to the theoretical model earlier developed by Ovchinnikov and Ivlev,²⁶ as extended by van der Beek *et al.*,²⁷ for the case of rather pure YBCO films containing sparse RE₂O₃ precipitates. They concluded that the strong pinning provided by sparse Y₂O₃ inclusions dominates over a broad temperature regime, thus

excluding weak collective pinning as the determinant of J_c . More recently, a strongly variable and temperature-dependent $\alpha \approx 0.48\text{--}0.94$ was reported for RE_2O_3 -containing films: α decreased with decreasing temperature and approached 0.5 at 5 K.²² By contrast a power-law, field-dependent J_c was observed at $T \leq 40$ K with $\alpha \approx 0.69$ at 5 K and 0.63 at 40 K for BZO-containing films.¹² The varied reports of these studies leave several unresolved questions. First, the $J_c(H\parallel c)$ relationship in Ovchinnikov and Ivlev's model does not predict a power-law function.²⁶ Second, it seems clear that there is no universal value for α from sample to sample, and indeed a power-law fit for $J_c(H)$ is not always valid. A third point is that α is often dependent on temperature, even for one particular sample, suggesting that the dominant pinning mechanism is temperature dependent. Fourth, it is especially clear from recent samples containing correlated pins that REBCO films are still on an increasing J_c and vortex pinning path and thus that the concept of a standard nanostructure with any so-called "standard pinning" is transitory and probably not very useful.^{13,14,28,29} Indeed we may note that the latest samples have bulk pinning force densities F_p that exceed by factors of $\sim 2\text{--}20$ the samples studied in Refs. 12, 21, 22, and 27. Thus a revisit of the wide range $J_c(\theta, H, T)$ characteristic of a modern very high J_c film is of both fundamental and practical interest.

Our viewpoint is that these new strong pinning films make it essential to accept that multiple types of pin are present and that it is reasonable to start with the common assumption that different pinning effects can be summed. Indeed Gutierrez *et al.*¹³ showed that the deconvolution of strong (as measured by their ability to still pin at high temperatures when thermal fluctuations are strong) from weak (thus capable of operating only at low temperatures) pinning effects in REBCO thin films containing big, sparse nanoparticles led to the conclusion that coexisting weak and strong pinning are both important for developing high J_c at low temperatures, a conclusion validated by other studies, too.^{22,23} But these studies still have not explored the magnetic field space at 10 T and above where YBCO can be so effective for magnet construction. It is this very high field regime up to ~ 30 T at 4.2 K that we study here, where thermal fluctuations are very much reduced. Compared to the usual higher temperature evaluation regimes, weak point pins can now greatly enhance J_c . BZO nanorod density seldom exceeds an equivalent vortex matching field B_ϕ of 2–3 T, making access to 20–30 T fields interesting because such fields vastly exceed any strong correlated vortex pin-vortex matching field. In particular, the low temperature pinning effect of BZO nanorods that are so effective at high temperatures needs experimental study for comparison to related theoretical work.^{6,30–33}

To address this need we here present the results of a systematic pinning physics study over a very broad magnetic field and temperature range on a recent REBCO thin film containing many types of defects. BZO nanorods, RE_2O_3 arrays, as well as a random distribution of RE_2O_3 nanoprecipitates were all observable by transmission electron microscopy (TEM). Based on extensive transport $J_c(\theta)$ data, we found that samples containing BZO nanorods show no signs of c -axis correlated pinning at 4.2 K, a result quite different from the strong c -axis correlated pinning that they show at higher temperatures. We conclude that additional uncorrelated

pinning not visible in the TEM examination greatly enhances J_c at 4.2 K and hides the correlated pinning of the nanorods. Indeed we find that this weak pinning adds significantly to the strong pinning and helps produce a record flux pinning force density $F_p > 900$ GN/m³ at 4.2 K. The dominant 4.2 K angular-dependent $J_c(\theta)$ characteristic, valid up to at least 31 T, can be fit to standard anisotropic mass scaling, except near the ab plane where correlated pinning, probably due to the CuO charge-reservoir layers, strongly enhances J_c . By measuring $J_c(\theta)$ over a wide range of field and temperature, we observe that this additional weak uncorrelated pinning is active only below ~ 30 K. We conclude that these low temperature, angular-independent pins are largely point pins induced by the strain fields of the BZO nanorods and, because they are point pins, they are easily thermally depinned at higher temperatures, leaving the strong correlated c -axis pinning effects of the BZO nanorods then quite evident. The net result of these multiple pin types is to produce strongly temperature-dependent pinning characteristics. The BZO nanorods, though not apparent at 4.2 K, nevertheless do still exert a strong effect on vortex pinning through their generation of point pinning centers which play a major role in driving the bulk pinning force density above 900 GN/m³ at 4.2 K. In this important respect the pinning effects are additive and of approximately equal importance at 4.2 K. Our analysis also suggests that the last word on raising J_c in REBCO thin films is very unlikely to have been yet spoken but also suggests that strategies for deconvoluting the different contributions to J_c will be valuable in the ongoing task of further improving the properties.¹³

II. EXPERIMENTAL DETAILS

We performed an extensive transport angular $J_c(\theta, T, H)$ characterization of a recent REBCO thin film in fields up to 31 T and temperatures from 4.2 to 77 K. The 1.1- μm -thick film (thickness verified by scanning electron microscopy) was grown by metal-organic chemical vapor deposition (MOCVD) on a high strength Hastelloy metal tape, on which a MgO buffer layer textured by ion-beam-assisted deposition (IBAD) was deposited. An $\sim 2\text{-}\mu\text{m}$ -thick sputtered silver layer was deposited on the REBCO layer as protection and an intermediate electrical contact layer over which an $\sim 50\text{-}\mu\text{m}$ -thick copper layer was electroplated.³⁴ This sample is representative of the most advanced coated conductor made by SuperPower Inc. The Zr addition produces BZO nanorods with an equivalent flux density $B_\phi \approx 2.6$ T. Earlier study has shown that such films have high J_c properties at both high and low temperatures.³⁵

The 4.2 K and high field four-probe critical current measurements were performed in a 52-mm cold bore 15 T superconducting magnet and a 52-mm warm bore 31 T Bitter magnet at the National High Magnetic Field Laboratory (NHMFL), fitted with a 38-mm bore liquid He cryostat. The 10–77 K measurements were carried out in a 16 T Physical Property Measurement System (PPMS). Samples were always rotated with respect to the external magnetic field around the axis parallel to the current direction to maintain a maximum Lorentz force configuration. The angle $\theta = 0$ is defined as the applied magnetic field perpendicular to the tape plane whose parallelism to the crystallographic c -axis direction has a typical

uncertainty of $1^\circ - 4^\circ$ produced by an offset caused by the IBAD process.³⁴⁻³⁶

Due to the high critical current I_c values observed at lower temperatures, samples with different geometries were prepared in order to avoid harmful Joule heating and overstressing by the large Lorentz forces ($I_c \times B$) possible in different regimes of temperature and magnetic field. A $50 \times 500\text{-}\mu\text{m}$ link was cut by a Nd-YAG (yttrium aluminum garnet) laser for the J_c measurement at 77 K. Even narrower samples, $\sim 10\ \mu\text{m}$ wide and $200\ \mu\text{m}$ long, were patterned by SEM/FIB so as to restrict I_c to $\sim 5\ \text{A}$ when the sample was measured in helium gas between 10 and 77 K. In both cases, copper and silver layers were removed by wet etching. Larger bridges about 1 mm wide and 1 cm long were patterned leaving the silver and copper layers present for the high current 4.2 K measurements. Two different home-made I_c probes equipped with rotating sample platforms were used. One had a maximum current-carrying capability of $\sim 500\ \text{A}$ for high I_c measurement in a liquid-helium bath, while the second had $\sim 5\ \text{A}$ capability in the gas-cooled PPMS cryostat for studies at temperatures above 10 K.

The critical temperature T_c is defined as the temperature where resistance equals zero. The 77 K irreversibility field was determined from the field dependence of J_c with the criterion $J_c = 100\ \text{A}/\text{cm}^2$. For lower temperatures where $H_{\text{irr}}(T)$ is greater than the magnetic field available, $H_{\text{irr}}(T)$ was assessed from the formula in Ref. 18:

$$H_{\text{irr}}^{\parallel c}(T) = H_0(T/T_c)^{-\alpha}(1 - T/T_c)^\beta \quad (1)$$

where H_0 , α , and β are determined experimentally to be 88 T, 0.15, and 1.15, respectively. TEM images were taken in a JEOL JEM 2011 transmission electron microscope.

III. RESULTS

The MOCVD thin film under study has a critical temperature $T_c = 90.7\ \text{K}$. The nominal composition of this sample is $\text{Y}_{0.6}\text{Gd}_{0.6}\text{Ba}_2\text{Cu}_{2.3}\text{O}_x$ with 7.5 at. % Zr doping, the composition found to give the highest in-field J_c values at 77 K.³⁴ At 77 K, the sample has $J_c = 3.4\ \text{MA}/\text{cm}^2$ at self-field and $1.0\ \text{MA}/\text{cm}^2$ at 1 T, at $\theta = 0^\circ$. Even more importantly, both the irreversibility field, $H_{\text{irr}} = 10.2\ \text{T}$, and the maximum flux pinning force density, $F_{p\ \text{max}} = 12\ \text{GN}/\text{m}^3$ along the c axis, are substantially higher than that of other REBCO films with similar thickness, $\sim 1\ \mu\text{m}$. Both parameters indicate that strong pins capable of resisting strong thermal fluctuations are present.

Figure 1 shows a typical cross-sectional, bright-field TEM image of this MOCVD thin film in which BZO nanorods, with $\sim 8\ \text{nm}$ diameter and inclinations of $5^\circ - 20^\circ$ to the c axis are quite obvious. Their density corresponds to a matching field $B_\phi = \phi_0/a^2 \sim 2.6\ \text{T}$, where $a \approx 28\ \text{nm}$ is the measured average distance between the BZO nanorods and $\phi_0 = h/2e \approx 2.1 \times 10^{-15}\ \text{Wb}$ is the flux quantum. Such nanorods are responsible for the broad J_c maxima observed at elevated temperatures when H is rotated towards the film plane perpendicular. This strong correlated pinning produces the outstanding superconducting performance observed at 77 K. Moreover, a high density of self-assembled RE_2O_3 precipitate arrays aligned along the ab plane is also visible in Fig. 1

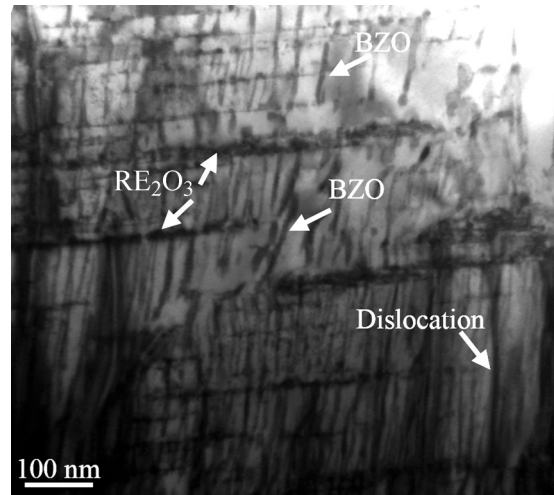


FIG. 1. (Color online) Cross-sectional TEM image of the MOCVD thin film. BZO nanorods inclined around the c axis and tilted RE_2O_3 precipitate arrays in the ab plane are the major visible correlated pinning centers. Additional random RE_2O_3 precipitates enhance J_c at all orientations. A low density of threading dislocations provides additional correlated pinning along the c axis.

and is another important source of strong, correlated pinning, in this case around the ab plane.^{11,18,36} Interestingly, TEM observation indicates that the ab plane of REBCO tilts $\sim 2^\circ$ from the buffer layer because of the IBAD texturing process, while the RE_2O_3 precipitate arrays tilt away from the ab plane by $\sim 5^\circ$, as previously reported.¹⁸ Threading dislocations provide additional c -axis correlated pinning, although we believe that their contribution is negligible compared to BZO nanorods because of their low density.

Figure 2(a) presents the c -axis field dependence $J_c(H\parallel c)$ for magnetic fields up to 16 or 31 T at various temperatures from 4.2 to 77 K. $J_c(H)$ shows less field dependence with decreasing temperature, as expected from the rapidly increasing $H_{\text{irr}}(T)$. At 10 K, J_c at self-field reaches $43\ \text{MA}/\text{cm}^2$, which corresponds to $\sim 17\%$ of the depairing current density J_d . J_c at 16 T and 10 K reaches $3.7\ \text{MA}/\text{cm}^2$, a value equal to the self-field J_c at 77 K. At 4.2 K, J_c decreases from $33.3\ \text{MA}/\text{cm}^2$ at 1 T to $2.9\ \text{MA}/\text{cm}^2$ at 31 T. These high current densities correspond to extremely high critical current $I_c > 1.5\ \text{kA}$ at 31 T and $H\parallel ab$ for standard production 4-mm-wide tape. Such high I_c and J_c values make effective measurement of $I_c(\theta, H)$ very difficult at low temperatures. Notably, this MOCVD BZO-containing sample shows higher J_c at all temperatures below $\sim 70\ \text{K}$ than optimized Nb-Ti wire evaluated at 4.2 K,³⁷ thus defining the opportunities for these new conductors for magnet construction. The power-law dependence of J_c on magnetic field, $J_c \propto H^{-\alpha}$, is observed at low temperatures. At 4.2 K, the power-law exponent $\alpha \approx 0.7$ describes J_c well in the whole 1–31 T range of magnetic field. It can easily be seen from Fig. 2(a) that α is strongly temperature dependent and that at higher temperatures it is doubtful that a power-law representation of J_c is warranted.

Figure 2(b) shows flux pinning force density $F_p = J_c \times \mu_0 H$ as a function of external magnetic field parallel to the c axis at various temperatures. The superior F_p values confirm the strong pinning provided by the defects existing in this

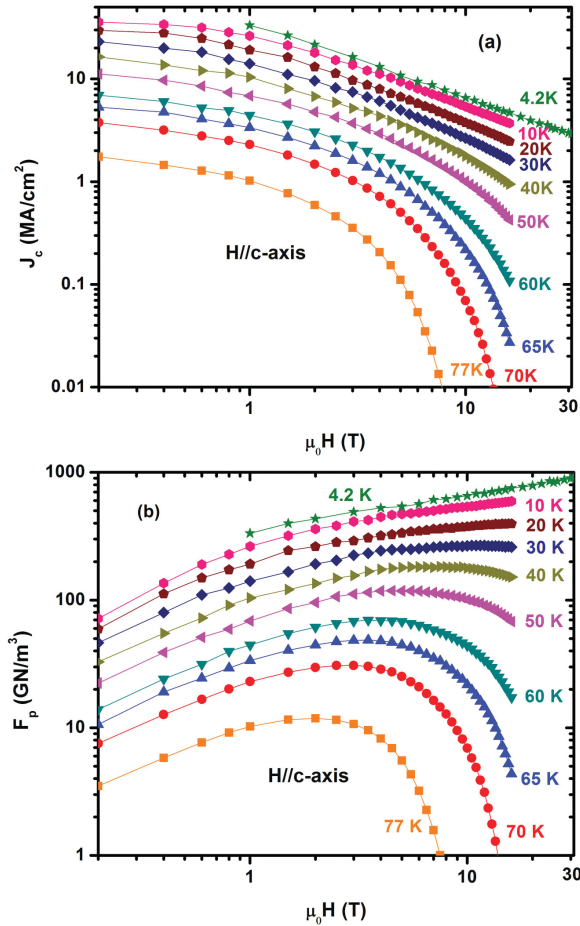


FIG. 2. (Color online) (a) Field dependence of J_c for H parallel to the c axis at temperatures between 4.2 and 77 K and magnetic fields up to 31 T. (b) The corresponding flux pinning force density calculated from $F_p = J_c \times \mu_0 H$. An excellent linear characteristic $J_c \propto H^{-\alpha}$ is observed at temperatures below ~ 30 K but such a power-law representation becomes increasingly less valid at higher T . It can be seen that $F_{p, \max}$ is trending to more than 1 TN/m^3 at $\mu_0 H > 31 \text{ T}$ at 4.2 K.

sample. The highest measured F_p at 4.2 K and 31 T almost reaches 1000 GN/m^3 . This is the highest value reported in any superconductor so far. It is also striking that the pinning force density above 4 T at 30 K barely depends on magnetic field. The maximum pinning force density is $\sim 267 \text{ GN/m}^3$ at 30 K, while at lower temperatures F_p maxima correspond to fields higher than 16 T (or even 31 T at 4.2 K) and could not be observed experimentally. The double-peaked $F_p(H)$ dependence shown by a recent BZO-doped YBCO film grown by pulsed laser deposition (PLD) on a SrTiO₃ single-crystal substrate³⁸ is not observed in the present work at any temperature.

The angular dependence of J_c is a powerful tool for understanding pinning mechanisms and also is crucial for magnet design because the magnetic field vector occupies all angles with respect to the tape plane somewhere in the winding. Figure 3 presents $J_c(\theta, 1, \text{ and } 4 \text{ T})$ at 77, 50, 30, and 10 K. J_c maxima around the c axis are clearly seen at 77 and 50 K. However, these maxima do not occur exactly at 0° due to the splayed inclination of the BZO nanorods. At 1 T and 77 K, the

c axis J_c reaches 1.1 MA/cm^2 , about one-third higher than the J_c maximum value around the ab plane and twice the minimum J_c close to the ab plane. As the magnetic field increases to 4 T, the c -axis J_c peak becomes lower than the ab peak, because the field exceeds the matching field of 2.6 T, corresponding to the BZO nanorod density. There is clearly a change in the angular pinning effectiveness as the vortex density starts to exceed the BZO pin density. It is worth noting too that both BZO nanorods and the RE₂O₃ precipitate arrays contribute to J_c at 77 K, BZO being responsible for the c -axis peak and the RE₂O₃ arrays for J_c enhancement over the whole angular range, especially around the ab plane. Comparing the 77 K $J_c(\theta)$ to lower temperature data at 1 and 4 T, the c -axis peak becomes less distinct as temperature decreases, not being observable at all at temperatures below ~ 30 K. This strongly suggests that the dominant pinning mechanisms change at lower temperatures and that the crossover temperature is ~ 30 K. It is striking that the ratio of $J_c \parallel c$ and $J_c \parallel ab$ decreases from 1.4 at 77 K to 0.9 at 50 K as the mass anisotropy reasserts its dominant role at lower temperatures and the $J_c \parallel ab$ peak becomes increasingly evident, indicating a strengthening of the ab -plane correlated pinning just as the c -axis correlated pinning disappears from evident view. At low fields, $J_c \parallel ab$ varies from a cusplike dependence above 50 K to a smooth, Ginzburg-Landau (GL)-like peak at lower temperatures and at 10 K from GL-like at low fields to cusplike at high magnetic fields.

Ultra-high-field magnet applications at 4.2 K are an important use of REBCO films, for which we have performed studies of $J_c(\theta)$ up to 31 T.^{35,36} Figure 4 shows the angular dependence of J_c of this MOCVD sample at 4.2 K up to 25 T. Evidently the c -axis J_c peak is totally washed out at 4.2 K at all fields from 3 up to 25 T. As noted also in the context of data taken at 10 K, the GL-like $J_c(\theta)$ dependence evolves towards a cusp for magnetic fields above ~ 5 T. In summary, the J_c data on this very strong pinning sample show a continuously evolving characteristic whose details and magnitude are very sensitive to field and temperature.

IV. DISCUSSION

The temperature and magnetic field dependence of the flux pinning force density for many superconductors often obeys a scaling relation, as was first proposed by Fietz and Webb:^{37,39}

$$F_p(T, H) = \text{const} \times [H_{c2}(T)]^n g(h) \quad (2)$$

in which the exponent n describes the temperature dependence of the upper critical field $H_{c2}(T)$ or, in this case, the irreversibility field $H_{\text{irr}}(T)$, and $g(h)$ is a pinning function which, in simple cases where the dominant pinning mechanisms are temperature independent, depends only on the reduced field h [$h = H/H_{\text{irr}}(T)$]. We first address the extent to which such a simple temperature-independent pinning assumption is valid for this strong pinning sample over the very broad range of T and H studied in this paper.

The reduced pinning force density $F_p/F_{p, \max}$ as a function of reduced magnetic field h is plotted in Fig. 5(a) using a reduced field defined as $h = H/H_{\text{irr}}(T)$, instead of $h = H/H_{c2}(T)$ for low temperature superconductors.³⁷ In both cases the aim is the same: the scaling field is defined for the field at which J_c tends to zero. At $T = 77 \text{ K}$, $F_p/F_{p, \max}$

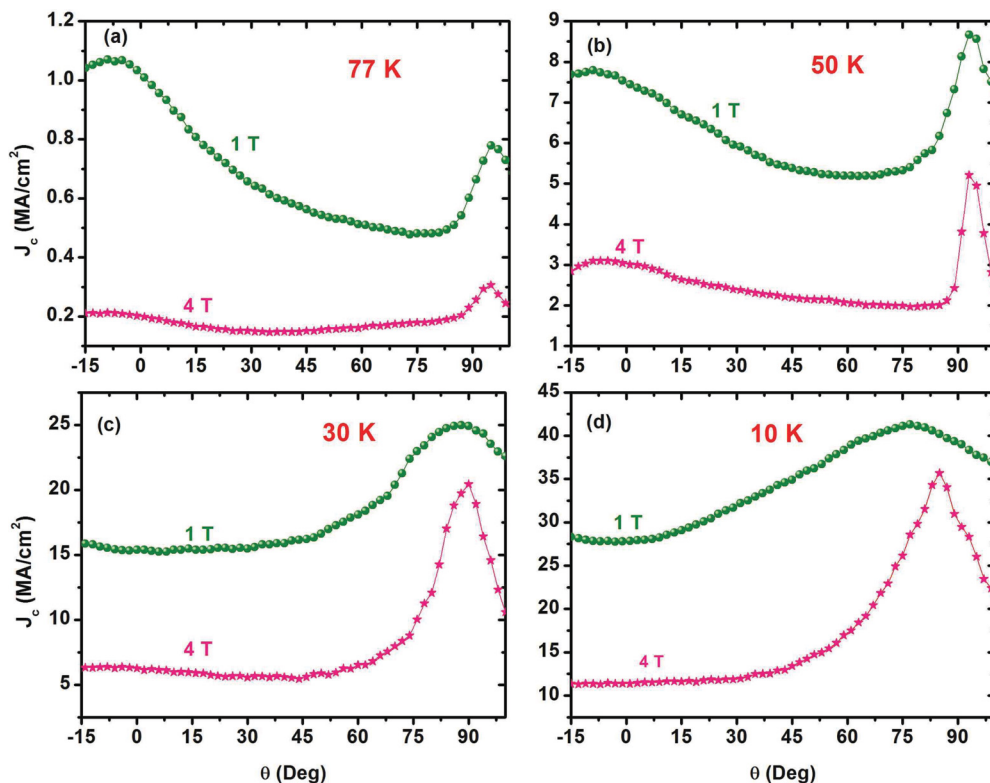


FIG. 3. (Color online) $J_c(\theta)$ at (a) 77, (b) 50, (c) 30, and (d) 10 K and magnetic fields up to 4 T. The c -axis J_c peak caused by the BZO nanorods is evident at 77 K and 1 T but becomes progressively less obvious with increasing magnetic field or decreasing temperature. Below 30 K, the peak is completely unobservable at any magnetic field.

peaks at $h = 0.2$ and $H = 2.0$ T, which is close to the matching field of 2.6 T for BZO nanorods in this sample. On decreasing temperature from 77 to 50 K, the peak h_{\max} shifts to lower reduced field, from 0.2 to 0.15, indicating that there is no simple correlation between h_{\max} and B_ϕ . With further temperature decrease to 30 K, there is no obvious change of the peak position. However, the pinning force peak width broadens as the temperature is lowered to 40 K and then to 30 K. Thus, exact temperature scaling does not occur in this sample, as is further demonstrated in Fig. 5(b) by plotting $\log_{10} F_p$ vs $\log_{10} H_{\text{irr}}(T)$ at varying reduced fields. The temperature scaling exponent n increases from 1.65 to 2.06 as the reduced field rises from 0.25 to 0.75. However, excellent temperature scaling is observed at constant reduced field, as shown by the linear dependence of $\log F_p$ on $\log H_{\text{irr}}(T)$. Taken together, both figures indicate that the dominant pinning mechanism(s) vary with temperature. The total pinning strength increases at lower temperatures even though the vortex density becomes much larger than the BZO nanorod correlated pinning density (2.6 T).

Additional compelling evidence for the temperature dependence of the pinning mechanisms is provided by the temperature dependence of J_c/J_d , the ratio of the measured pinning critical current density to the calculated depairing current density, which may be used as a convenient measure of the effectiveness of the pinning defects in the phenomenology of type II superconductors.⁶ In this work, we use J_c/J_d to track the pinning strength variation with temperature. Figure 6 presents J_c/J_d for H parallel to the c axis as a function of

temperature at several different magnetic fields, where J_d is obtained from the following equation:^{40,41}

$$J_d(T, H) = J_d(T = 0, H = 0) \left(1 - \frac{T}{T_c}\right)^{3/2} \left(1 - \frac{H}{H_{c2}(T)}\right)^{3/2} \quad (3)$$

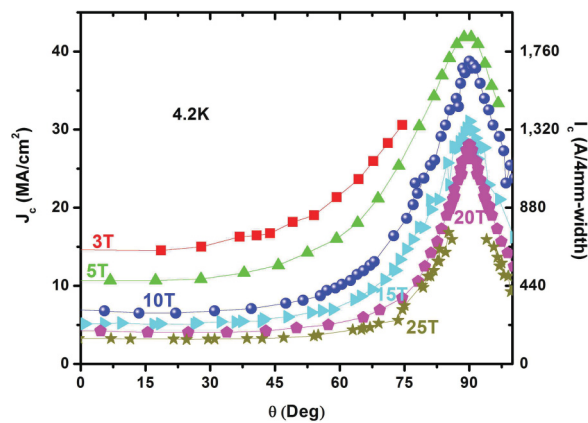


FIG. 4. (Color online) $J_c(\theta)$ at 4.2 K under magnetic fields up to 25 T. The c -axis J_c peak is totally absent, while the J_c peak around the ab plane becomes narrower at higher field. It is also significant that this BZO-containing thin film shows higher J_c and a broader J_c maximum around the ab plane than similar samples without BZO nanorods (Refs. 35 and 36).

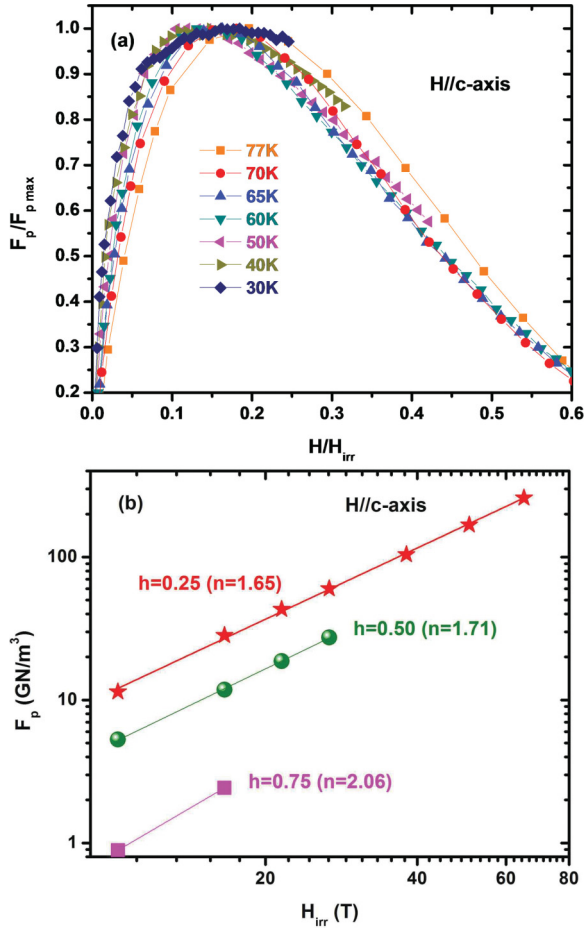


FIG. 5. (Color online) (a) Reduced pinning force density $F_p/F_{p \max}$ for H parallel to the c axis as a function of reduced magnetic field H/H_{irr} at temperatures from 30 to 77 K. The curves do show a lack of a perfect temperature scaling of F_p . (b) F_p as a function of irreversibility field at several reduced magnetic fields does show good temperature scaling at constant reduced field, but the exponent rises with increasing field.

Here $J_d(0,0) = 300 \text{ MA/cm}^2$ taking $\xi_{ab}(0) = 1.2 \text{ nm}$, $\lambda_{ab}(0) = 170 \text{ nm}$,⁴¹ and $H_{c2}(T) = H_{c2}(0)[1 - (T/T_c)^2]$. $T_c = 91 \text{ K}$ and $H_{c2}(0, H \parallel c) = 121 \text{ T}$.⁴² In the more often used self-field limit, this expression reduces to the usual equation $J_d = \phi_0/3\sqrt{3}\pi\mu_0\lambda^2\xi$.

Two evident features are observed in Fig. 6. First, it is clear that the ratio J_c/J_d continuously declines with increasing temperature for all fields from 1 to 16 T, signaling that at least some portion of the pinning is sensitive to thermal fluctuations, even in this strong pinning regime.^{43–46} At the lowest field evaluated, 1 T, it appears that three temperature regimes can be distinguished. On raising the temperature from 4.2 to about 30 K, there is an initially steep drop of J_c/J_d , the rate of decrease then flattening between about 30 and 65 K, before finally accelerating again as thermal fluctuations dominate at the highest temperatures. The strong thermal fluctuation regime seems to start at $\sim 65 \text{ K}$ at 1 T, 60 K at 4 T, 50 K at 8 T, and 40 K at 16 T. The initially steeper, low temperature fall in J_c/J_d quite visible in the 1–4 T curves suggests an additional pinning mechanism operating only at low temperatures. However, the contribution of this pinning

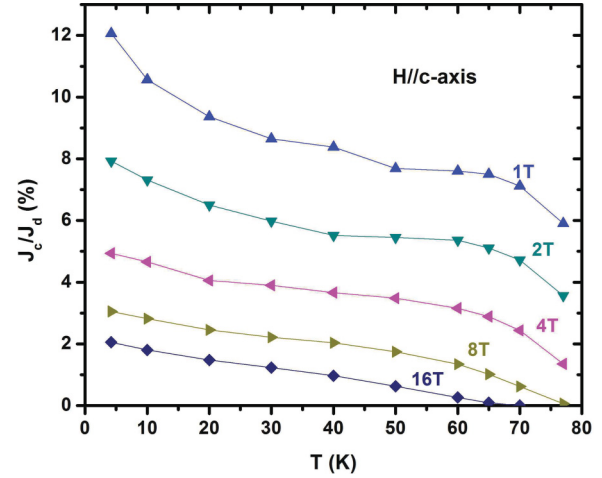


FIG. 6. (Color online) The ratio of transport and depairing current densities J_c/J_d for H parallel to the c axis as a function of temperature at fields of 1–16 T. Three temperature regimes of J_c/J_d are visible. Starting from low temperature, J_c/J_d falls steeply before moderating between ~ 30 to 60 K (at 1 T), then falling again very steeply at ~ 60 –80 K.

mechanism is degraded by both increasing temperature and increasing field, so that at 16 T its effect is only weakly visible as a point of inflection at 10–15 K on the $J_c/J_d(T)$ plot.

More details can be obtained by plotting $\log J_c$ vs T and $\log J_c$ vs T^2 . Flux pinning can be categorized as strong or weak based on the extent of the distortion of the flux line lattice by the pinning defects. It has been shown that the J_c determined by weak pinning decays exponentially with temperature, while J_c arising from strong pinning decays as an exponential function of T^2 .^{22,23,46–48}

$$J_c^{\text{wk}}(T) \approx J_{c0}^{\text{wk}} \exp \left[- \left(\frac{T}{T_0^{\text{wk}}} \right) \right] \quad (4)$$

$$J_c^{\text{str}}(T) \approx J_{c0}^{\text{str}} \exp \left[-3 \left(\frac{T}{T_0^{\text{str}}} \right)^2 \right] \quad (5)$$

where J_{c0}^{wk} and J_{c0}^{str} are the contributions to J_c at 0 K of weak and strong pinning defects, respectively, and T_0^{wk} and T_0^{str} describe their characteristic pinning energies. Accordingly, Fig. 7(a) plots $\log J_c$ vs T^2 . J_c indeed decays as an exponential function of T^2 in the intermediate temperature regime of 30–65 K at 1 T, 30–60 K at 4 T, 30–50 K at 8 T and 12 T, but it is also clear that there is an “excess” J_c at the lowest temperatures which quickly disappears at higher temperatures. At lower temperatures, as shown in Fig. 7(b), the exponential decay of J_c , shown by the linear dependence of $\log J_c$ on T , is observed below $\sim 40 \text{ K}$ at 1 and 4 T and below $\sim 30 \text{ K}$ at 8 and 12 T. This analysis also points to the appearance of additional weak pinning below $\sim 30 \text{ K}$, as also noted elsewhere in the literature,^{21,27} but only at very low magnetic field in the single vortex regime $\mu_0 H < 0.2 \text{ T}$. In the ~ 30 –60 K range, stronger pinning centers then control J_c until even these strong pins are rendered ineffective by increasing thermal fluctuations close to T_c . The strong pinning provided by the BZO nanorods and RE_2O_3 precipitates in this sample significantly raises the crossover temperature beyond which thermal fluctuations dominate to $\sim 60 \text{ K}$, as compared

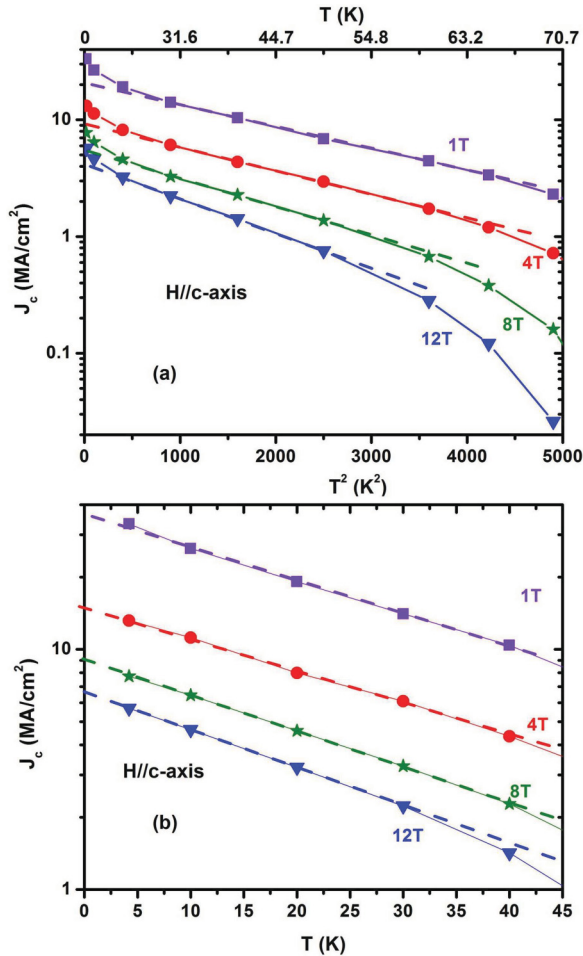


FIG. 7. (Color online) Plot of (a) $\log J_c$ vs T^2 and (b) $\log J_c$ vs T for H parallel to the c axis. A linear dependence of $\log J_c$ on T^2 characteristic of strong pinning is observed in the intermediate temperature range ~ 30 – 60 K in (a) while the linear dependence of $\log J_c$ on T characteristic of weak pinning is observed at temperatures below ~ 30 K in (b). Taken together the plots indicate that dense weak pinning adds to the strong pinning provided by RE_2O_3 and BZO nanorods up to about 30 K and that strong pins then dominate J_c until strong thermal fluctuations start to degrade J_c above ~ 65 K (at 1 T).

to ~ 30 K in YBCO single-crystal samples where few if any strong pins are present.⁴⁵ The BZO nanorods and RE_2O_3 precipitates provide strong pinning at ~ 30 – 60 K, as clearly shown by multiple other studies.^{13,28,48}

Further information about the additional low temperature weak pinning can be obtained by analysis of the angular dependence of J_c at 4.2 K using the anisotropic scaling approach proposed by Civalè *et al.*⁴⁹ If the pinning is due to uncorrelated defects randomly distributed over angular space, then J_c should depend on H and θ only through a single variable $J_c(H, \theta) = J_c[H\varepsilon(\theta)]$, where $\varepsilon(\theta) = [\cos^2(\theta) + \gamma^{-2}\sin^2(\theta)]^{1/2}$ and γ^2 is the electronic mass anisotropy parameter. Since we have observed that J_c for $H||c$ follows $J_c \propto H^{-\alpha}$ at low temperatures, especially at 4.2 K [as shown in Fig. 2(a)], then $J_c(H, \theta) \propto [H\varepsilon(\theta)]^{-\alpha}$. Power-law behavior with $\alpha \approx 0.7$ for BZO-containing samples and $\alpha \approx 0.5$ for non-BZO samples was reported by us previously.³⁵ Figure 8 presents $J_c(\theta)$ at 5, 15, and 25 T using the anisotropic scaling

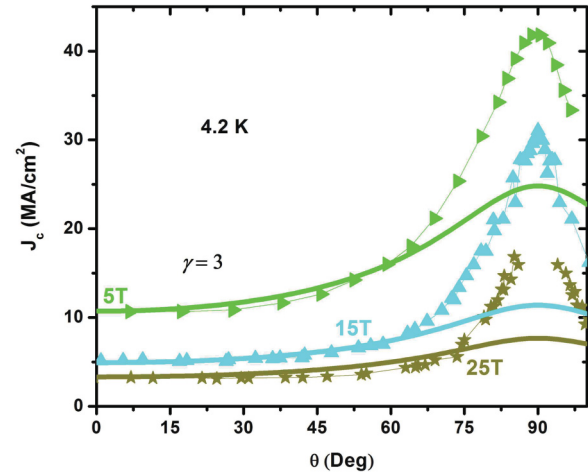


FIG. 8. (Color online) Angular dependence of J_c (symbols) and J_c calculated from anisotropic G-L scaling model (thick lines) at 4.2 K and magnetic fields 5, 15, and 25 T. Anisotropic G-L scaling describes well the experimental data over a broad angular range, ~ 0 – 60° with $\alpha = 0.7$ and $\gamma = 3$. Thus, weak uncorrelated pinning contributes greatly to J_c at 4.2 K except in the vicinity of the ab plane where intrinsic pinning dominates compared to pinning by RE_2O_3 precipitates and stacking faults.

parameters $\alpha = 0.7$ and $\gamma = 3$. These curves give a reasonable fit of the data in the low temperature region from 0° up to about 60 – 70° , leading us to conclude that over a wide angular range about the c axis (where the correlated effects of the BZO nanoparticles are so evident at higher temperatures), the pinning is indeed uncorrelated and random. Clearly the most reasonable interpretation of this behavior is that the additional pinning that operates only up to 30 – 40 K hides the strong pinning effect of the BZO nanorods at lower temperatures. It is interesting that the scaling suggests an effective anisotropy $\gamma = 3$, somewhat smaller than the H_{c2} anisotropy $\gamma = 5$ expected from the intrinsic mass anisotropy $\gamma^2 = 25$ – 30 . It is interesting that $\gamma = 3$ was also deduced from a very broad study of the angular variation of $H_{\text{irr}}(T)$ for a very similar sample over the range ~ 55 – 80 K and H up to 45 T.⁵⁰ In this case the effective γ was evaluated in the limit of H_{irr} when the pin strength goes to zero, rather than in the very finite pin strength limit assessed here, implying a rather consistent behavior over a wide range of the superconducting phase space. Evidently pinning centers lessen the effective anisotropy below the intrinsic mass anisotropy, no doubt by imposing a preferred angular alignment of vortices over a wide range of T and H , an outcome that is broadly positive for applications.

The power-law dependence of J_c on H has been reported in many works.^{22,28,51} However, the increase of α from 0.5 (no nanorods) to 0.7 at 4.2 K when BZO nanorods are present is in contrast to high temperature observations where the presence of BZO nanorods markedly decreases α due to their strong pinning effect.^{28,35} This is yet more evidence that different pinning mechanisms operate at high and low temperatures.

Based on the above analysis, we propose that BZO additions lead to a significant density of strain-induced, weak pins that cannot resist thermal fluctuations much above about 30 K. Since they do operate at all fields up to 31 T at 4.2 K, it is clear

that they are much denser than the strong BZO and RE₂O₃ pins. However, they are also susceptible to weakening by increasing field and temperature, consistent with our deduction that these are point pins (effective size of order ξ^3 or less, where ξ is the coherence length). Our earlier 4.2 K comparison of non-BZO and BZO-containing samples up to 31 T showed two significant features: One was that the BZO samples have significantly higher J_c than equivalent films made without BZO, while the second was that the enhancement disappeared by 30–35 T, certainly a high field but actually only about 25% of H_{irr} or H_{c2} at 4.2 K. Here our variable temperature examination of the BZO sample shows that the uncorrelated pinning effects produced by the point pins are only visible up to ~ 30 K. Both characterizations show that the pin strength decays rapidly with increasing H and T , consistent with them being small and easily thermally depinned. As Fig. 1 shows, only the larger BZO and RE₂O₃ strong pins are visible in TEM, so we do not yet have a measure of the point pin concentration. But we can reasonably infer that their density must be high, since they are able to completely hide the effect of the BZO nanorods, even at fields below B_ϕ [compare the $J_c(1\text{ T})$ data at 77 and 10 K in Figs. 3(a) and 3(d)]. Indeed, the depressed T_c of MOCVD and PLD REBCO samples induced by BZO nanorods has recently been attributed to oxygen deficiencies introduced by strain imposed by the lattice mismatch between BZO nanorods and the REBCO matrix.⁵² Specific supporting evidence was provided by atomic-resolution Z -contrast imaging and electron energy loss spectroscopy which showed oxygen deficiencies surrounding BZO nanorods, a finding entirely consistent with our proposal for dense point pins. Cantoni's work also shows that the microstrain in the pure MOCVD thin films without BZO nanorods is $\sim 0.15\%$, and that it increases with the BZO concentration.⁵² Thus the overall conclusion of our study is extremely positive: the splayed BZO nanorods that provide strong correlated pinning around the c axis in the 50–77 K range also greatly add to the lower temperature J_c by inducing strain-induced point defects

that raise J_c in the whole angular range at fields up to at least 31 T at 4.2 K where thermal depinning effects are small.

V. CONCLUSIONS

In this paper, we presented a very detailed $J_c(H, T, \theta)$ characterization of a modern, very high critical current density REBCO thin film containing $\sim c$ -axis-oriented BZO nanorods and ab -plane RE₂O₃ pinning arrays over an exceptionally broad temperature (4.2–77 K) and magnetic field range (0–31 T). By analyzing the J_c data we studied the field- and temperature-dependent pinning evolution. An important new conclusion is that uncorrelated pinning from point defects produced by the strain field around BZO nanorods dominates J_c at low temperatures. More specifically, we observed that the usual c -axis J_c peak caused by BZO nanorods disappears with decreasing temperature, and vanishes completely below ~ 30 K. At 4.2 K, we found that J_c along the c axis decays as $J_c \propto H^{-\alpha}$ with magnetic field up to 31 T. Although $J_c(H)$ decays faster at 4.2 K compared to samples without BZO nanorods, J_c remains higher at fields up to at least 31 T, consistent with extra pinning induced by the BZO nanorods. At low temperatures, the c -axis J_c peak is not seen at any magnetic field and the only correlated pinning occurs around the ab plane.

ACKNOWLEDGMENTS

We are very grateful to colleagues in the HTS R&D group at the NHMFL who have provided many valuable comments and discussions, especially Dima Abraimov, Alex Gurevich, David Hilton, Fumitake Kametani, Chiara Tarantini, John Sinclair, and Huub Weijers. Earlier portions of this work were supported by the Department of Energy, Office of Electric Delivery and Energy Research (Grant No. DE-FC07-08ID14916), and some by the National High Magnetic Field Laboratory, which is supported by NSF Cooperative Agreement DMR-0654118 and by the State of Florida.

*aixiaxu@asc.magnet.fsu.edu

¹D. C. Larbalestier, A. Gurevich, D. M. Feldmann, and A. Polyanski, *Nature (London)* **414**, 368 (2001).

²J. Hua, U. Welp, J. Schlueter, A. Kayani, Z. L. Xiao, G. W. Crabtree, and W. K. Kwok, *Phys. Rev. B* **82**, 024505 (2010).

³H. Weijers, U. Trociewitz, W. Markiewicz, J. Jiang, D. Myers, E. Hellstrom, A. Xu, J. Jaroszynski, P. Noyes, Y. Viouchkov, and D. C. Larbalestier, *IEEE Trans. Appl. Supercond.* **20**, 576 (2010).

⁴S. R. Foltyn, L. Civale, J. L. MacManus-Driscoll, Q. X. Jia, B. Maiorov, H. Wang, and M. Maley, *Nature Mater.* **6**, 631 (2007).

⁵T. G. Holesinger, L. Civale, B. Maiorov, D. M. Feldmann, J. Y. Coulter, D. J. Miller, V. A. Maroni, Z. Chen, D. C. Larbalestier, R. Feenstra, X. Li, Y. Huang, T. Kodankandath, W. Zhang, M. W. Rupich and A. P. Malozemoff, *Adv. Mater.* **20**, 391 (2008).

⁶G. Blatter, M. V. Feigel'man, V. B. Geshkenbein, A. I. Larkin, and V. M. Vinokur, *Rev. Mod. Phys.* **66**, 1125 (1994).

⁷C. Jooss, R. Warthmann, H. Kronmüller, T. Haage, H.-U. Habermeier, and J. Zegenhagen, *Phys. Rev. Lett.* **82**, 632 (1999).

⁸W. D. Markiewicz, H. W. Weijers, P. D. Noyes, U. P. Trociewitz, K. W. Pickard, W. R. Sheppard, J. J. Jaroszynski, A. Xu, D. C. Larbalestier, and D. W. Hazelton, AIP Conf. Proc. No. 1218 (AIP, Melville, NY, 2010), p. 225.

⁹U. P. Trociewitz, M. Dalban-Canassy, M. Hannion, D. K. Hilton, J. Jaroszynski, P. Noyes, Y. Viouchkov, H. W. Weijers, and D. C. Larbalestier, *Appl. Phys. Lett.* **99**, 202506 (2011).

¹⁰T. Haugan, P. N. Barnes, R. Wheeler, F. Meisenkothen, and M. Sumption, *Nature (London)* **430**, 867 (2004).

¹¹X. Song, Z. Chen, S. Kim, D. M. Feldmann, D. Larbalestier, J. Reeves, Y. Xie, and V. Selvamanickam, *Appl. Phys. Lett.* **88**, 212508 (2006).

¹²M. Miura, B. Maiorov, S. A. Baily, N. Haberkorn, J. O. Willis, K. Marken, T. Izumi, Y. Shiohara, and L. Civale, *Phys. Rev. B* **83**, 184519 (2011).

¹³J. Gutiérrez, A. Lordés, J. Gázquez, M. Gibert, N. Romà, S. Ricart, A. Pomar, F. Sandiumenge, N. Mestres, T. Puig, and X. Obradors, *Nature Mater.* **6**, 367 (2007).

- ¹⁴J. L. MacManus-Driscoll, S. R. Foltyn, Q. X. Jia, H. Wang, A. Serquis, L. Civale, B. Maiorov, M. E. Hawley, M. P. Maley, and D. E. Peterson, *Nature Mater.* **3**, 439 (2004).
- ¹⁵S. A. Harrington, J. H. Durrell, B. Maiorov, H. Wang, S. C. Wimbush, A. Kursumovic, J. H. Lee, and J. L. MacManus-Driscoll, *Supercond. Sci. Technol.* **22**, 022001 (2009).
- ¹⁶L. Civale, B. Maiorov, M. Feldmann, and T. Holesinger, High Temperature Superconductivity Program Peer Review (Alexandria, VA), August 4–6, 2009, <http://www.htspeerreview.com/2009/pdfs/presentations/day%203/strategic-research/3-Strategic-Coated-Conductor-Performance.pdf>.
- ¹⁷S. H. Wee, A. Goyal, Y. L. Zuev, C. Cantoni, V. Selvamanickam, and E. D. Specht, *Appl. Phys. Express* **3**, 023101 (2010).
- ¹⁸Z. Chen, F. Kametani, Y. Chen, Y. Xie, V. Selvamanickam, and D. C. Larbalestier, *Supercond. Sci. Technol.* **22**, 055013 (2009).
- ¹⁹E. D. Specht, A. Goyal, J. Li, P. M. Martin, X. Li, and M. W. Rupich, *Appl. Phys. Lett.* **89**, 162510 (2006).
- ²⁰S. H. Wee, E. D. Specht, C. Cantoni, Y. L. Zuev, V. Maroni, W. Wong-Ng, G. Liu, T. J. Haugan, and A. Goyal, *Phys. Rev. B* **83**, 224520 (2011).
- ²¹A. O. Ijaduola, J. R. Thompson, R. Feenstra, D. K. Christen, A. A. Gapud, and X. Song, *Phys. Rev. B* **73**, 134502 (2006).
- ²²O. Polat, J. W. Sinclair, Y. L. Zuev, J. R. Thompson, D. K. Christen, S. W. Cook, D. Kumar, Y. Chen, and V. Selvamanickam, *Phys. Rev. B* **84**, 024519 (2011).
- ²³J. Plain, T. Puig, F. Sandiumenge, X. Obradors, and J. Rabier, *Phys. Rev. B* **65**, 104526 (2002).
- ²⁴B. Dam, J. M. Huijbregtse, F. C. Klaassen, R. C. F. van der Geest, G. Doornbos, J. H. Rector, A. M. Testa, S. Freisem, J. C. Martinez, B. Stäuble-Pümpin, and R. Griessen, *Nature (London)* **399**, 439 (1999).
- ²⁵F. C. Klaassen, G. Doornbos, J. M. Huijbregtse, R. C. F. van der Geest, B. Dam, and R. Griessen, *Phys. Rev. B* **64**, 184523 (2001).
- ²⁶Y. N. Ovchinnikov and B. I. Ivlev, *Phys. Rev. B* **43**, 8024 (1991).
- ²⁷C. J. van der Beek, M. Konczykowski, A. Abal’oshev, I. Abal’osheva, P. Gierlowski, S. J. Lewandowski, M. V. Indenbom, and S. Barbanera, *Phys. Rev. B* **66**, 024523 (2002).
- ²⁸B. Maiorov, S. A. Baily, H. Zhou, O. Ugurlu, J. A. Kennison, P. C. Dowden, T. G. Holesinger, S. R. Foltyn, and L. Civale, *Nature Mater.* **8**, 398 (2009).
- ²⁹P. Mele, K. Matsumoto, T. Horide, A. Ichinose, M. Mukaida, Y. Yoshida, S. Horii, and R. Kita, *Supercond. Sci. Technol.* **21**, 032002 (2008).
- ³⁰J. P. Rodriguez, P. N. Barnes, and C. V. Varanasi, *Phys. Rev. B* **78**, 052505 (2008).
- ³¹D. R. Nelson and V. M. Vinokur, *Phys. Rev. B* **48**, 13060 (1993).
- ³²D. R. Nelson and V. M. Vinokur, *Phys. Rev. Lett.* **68**, 2398 (1992).
- ³³D. C. Larbalestier, D. Abraimov, and A. Gurevich, Advanced Cables and Conductors Program Peer Review (Alexandria, VA), June 29–July 1, 2010, http://www.htspeerreview.com/pdfs/presentations/day%202/strategic-research/1_SR_CurrentLimiting-MechanismStudiesofCoatedConductors.pdf.
- ³⁴V. Selvamanickam, Y. Chen, I. Kesgin, A. Guevara, T. Shi, Y. Yao, Y. Qiao, Y. Zhang, Y. Zhang, G. Majkic, G. Carota, A. Rar, Y. Xie, J. Dackow, B. Maiorov, L. Civale, V. Braccini, J. Jaroszynski, A. Xu, D. C. Larbalestier, and R. Bhattacharya, *IEEE Appl. Supercond.* **21**, 3049 (2011).
- ³⁵V. Braccini, A. Xu, J. Jaroszynski, Y. Xin, D. C. Larbalestier, Y. Chen, G. Carota, J. Dackow, I. Kesgin, Y. Yao, A. Guevara, T. Shi, and V. Selvamanickam, *Supercond. Sci. Technol.* **24**, 035001 (2011).
- ³⁶A. Xu, J. Jaroszynski, F. Kametani, Z. Chen, D. C. Larbalestier, Y. L. Viouchkov, Y. Chen, Y. Xie, and V. Selvamanickam, *Supercond. Sci. Technol.* **23**, 014003 (2010).
- ³⁷C. Meingast and D. C. Larbalestier, *J. Appl. Phys.* **66**, 5971 (1989).
- ³⁸A. Augieri, G. Celentano, V. Galluzzi, A. Mancini, A. Rufoloni, A. Vannozzi, A. A. Armenio, T. Petrisor, L. Ciontea, S. Rubanov, E. Silva, and N. Pompeo, *J. Appl. Phys.* **108**, 063906 (2010).
- ³⁹W. A. Fietz and W. W. Webb, *Phys. Rev.* **178**, 657 (1969).
- ⁴⁰R. G. Boyd, *Phys. Rev.* **145**, 255 (1966).
- ⁴¹W. Lang, I. Puica, K. Siraj, M. Peruzzi, J. Pedarnig, and D. Buerle, *Physica C* **460-462**, 827 (2007).
- ⁴²T. Sekitani, N. Miura, S. Ikeda, Y. Matsuda, and Y. Shiohara, *Physica B* **346-347**, 319 (2004).
- ⁴³J. Vargas and D. C. Larbalestier, *Appl. Phys. Lett.* **60**, 1741 (1992).
- ⁴⁴A. Gurevich, *Supercond. Sci. Technol.* **20**, S128 (2007).
- ⁴⁵M. V. Feigel’man and V. M. Vinokur, *Phys. Rev. B* **41**, 8986 (1990).
- ⁴⁶S. Senoussi, M. Osséna, G. Collin, and I. A. Campbell, *Phys. Rev. B* **37**, 9792 (1988).
- ⁴⁷D. K. Christen and R. Thompson, *Nature (London)* **364**, 98 (1993).
- ⁴⁸T. Puig, J. Gutierrez, A. Pomar, A. Llord, J. Gzquez, S. Ricart, F. Sandiumenge, and X. Obradors, *Supercond. Sci. Technol.* **21**, 034008 (2008).
- ⁴⁹L. Civale, B. Maiorov, A. Serquis, J. O. Willis, J. Y. Coulter, H. Wang, Q. X. Jia, P. N. Arendt, M. Jaime, J. L. MacManus-Driscoll, M. P. Maley, and S. R. Foltyn, *J. Low Temp. Phys.* **135**, 87 (2004).
- ⁵⁰C. Tarantini, J. Jaroszynski, F. Kametani, Y. L. Zuev, A. Gurevich, Y. Chen, V. Selvamanickam, D. C. Larbalestier, and D. K. Christen, *Phys. Rev. B* **84**, 224514 (2011).
- ⁵¹Y. L. Zuev, D. K. Christen, S. H. Wee, A. Goyal, and S. W. Cook, *Appl. Phys. Lett.* **93**, 172512 (2008).
- ⁵²C. Cantoni, Y. Gao, S. H. Wee, E. D. Specht, J. Gazquez, J. Meng, S. J. Pennycook, and A. Goyal, *ACS Nano* **5**, 4783 (2011).